The superconductor-insulator transition in InO nanowires

Shachaf Poran, Department of physics, Bar Ilan University, Ramat-Gan, Israel

December 6, 2010

Abstract

The disorder-induced superconductor-insulator transition (SIT) is a transition between a superconducting and an insulating ground states of a system which occurs when a large amount of disorder is introduced to some superconductive materials. This transition has attracted a lot of attention both theoretically and experimentally during the the last 30 years and though much work and effort have been invested in measuring and quantifying this phenomenon there is no complete understanding of this subject.

Two main classes of the SIT have been traditionally explored: one being the SIT of a granular film and the other of a continuous film. The existence of a third class of materials which are fabricated structurally homogeneous but show signs of electrical inhomogeneity is the subject of an ongoing debate regarding the origin of this granularity.

This work focuses on extremely narrow wires (nanowires) of amorphous InO, a material which belongs to the third class. Nanowires having different geometries and levels of disorder were fabricated by means of e-beam lithography. Transport and magnetotransport measurements were performed on the nanowires at temperatures down to $300mK$ and magnetic fields up to $6T$.

A number of striking phenomena are observed in our nanowires. The most striking and surprising phenomenon is the appearance of a spontaneous voltage drop along the wire. This voltage appears only at intermediate degrees of disorder, namely when signs for superconductivity are observed but the wire is not fully superconducting, and at temperatures lower than T_c. This voltage also shows an antisymmetric dependence on magnetic field. The voltage versus field curve initially rises, reaches a maximum value and then decreases with a superimposed quasi-period. We discuss different possible origins for these effects, which include thermopower, Nernst effect, phase slips, external noise rectification etc.

We suggest that the most suitable explanation for this effect is a spontaneous appearance of the ratchet effect, in which vortices have a preferred direction of movement due to an asymmetric shape of pinning sites. This preferred direction alongside with alternating currents through the wire create a net movement of vortices across the wire, which translates into a voltage along the wire. In past explored systems the asymmetric shapes were intentionally fabricated to enforce this effect, however in our system this effect arises due to the presence of disorder which is random in space. This is another manifestation of the material's electrical inhomogeneity. A thorough description of how the effect fits our data is given in this work.

Contents

1 Theoretical overview **3**

1.1 Anderson insulators 3

1.2 Superconductors 6

1.3 Superconductor-insulator transition 16

2 Research goal **24**

3 Experimental **25**

3.1 Indium Oxide 25

3.2 Sample preparation 26

3.3 Measurements 28

4 Results **32**

4.1 Resistance of nanowires 33

4.2 Voltage along nanowires 35

5 Discussion **51**

5.1 Voltage along nanowire 51

6 Conclusion **58**

A Abbreviations **I**

Chapter 1

Theoretical overview

1.1 Anderson insulators

The classical Drude model [1], where the cause of electrical resistance is the electron's collisions with ions, held until the discovery of quantum mechanics and the evolution of Bloch's model of crystalline conductors [2]. Bloch's theory described an electron in a periodic potential as having an extended wave function which enables it to propagate throughout the crystal and thus participate in electric conduction. None of these models was sufficient when the potential of the system was not periodic, as is the case in disordered systems.

In 1958 [3] P.W Anderson predicted the existence of localization of electrons in disordered materials. He argued that adding a random potential to a crystal's periodic potential might not only decrease the electron's mean free path, but traps the electron in a localization site of finite size when the disorder is large enough, turning the medium into an electrical insulator. This happens since each potential well modified by disorder has its own energy spectrum, which makes tunneling from one site to the other improbable. Around those wells, called localization sites, the electron's wave function decays exponentially with a characteristic site size of ξ, which is known as the localization length. The electron wave function is given by $\Psi(r) \propto e^{-\frac{r}{\xi}}$ where r is the distance from the localization site's center. A sketch of a wave function in a disordered medium is shown in figure 1.1.

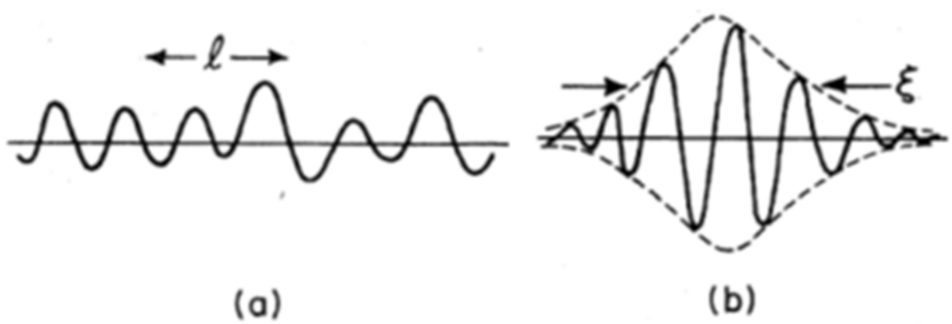

Figure 1.1: *(a) An extended electron wave function in a medium with weak disorder. (b) A localized electron wave function in a medium with strong disorder, showing localization in a site of characteristic size of ξ.*

In a typical electronic system many localization sites are distributed in space. This enables conduction through the disordered matter even in the presence of Anderson localization. For temperatures greater than zero an electron can tunnel from one potential well to the other and simultaneously lose or gain energy by emitting or absorbing a phonon, thus tunneling between states that do not have matching energies. This process is called "hopping". In zero temperature the conduction via this mechanism vanishes since phonons are unavailable. The conduction between two localization sites is given by

$$\sigma \propto e^{-\frac{2R}{\xi}-\frac{\Delta E}{kT}} \tag{1.1}$$

where ΔE is the average difference in energy levels between two sites, k is Boltzmann's constant and R the average distance between two grains.

About a decade after Anderson proposed his theory of localization, N.F. Mott [4] optimized Eq. 1.1 and found that this kind of conduction, called "Variable Range Hopping", is given by

$$\sigma \propto e^{-(\frac{T_0}{T})^{\frac{1}{d+1}}} \tag{1.2}$$

where d is the system's dimensionality and T_0 is a constant that depends on the density of states (DOS) at the Fermi level. The non-Ahrrhenius behavior of Eq. 1.2 is taken as a fingerprint of conduction in disordered systems which is not characterized by a well-defined energy barrier.

Efros and Shklovskii suggested [5] that in a localized medium the Coulomb interactions between electrons play an important role. A soft gap, known as the coulomb gap, appears in the DOS in such systems which lowers the conductivity. They showed that in the presence of such a gap a global conductance behavior is achieved, ignorant to the dimensionality of the system, which follows

$$\sigma \propto e^{-(\frac{T_0}{T})^{\frac{1}{2}}} \tag{1.3}$$

1.2 Superconductors

1.2.1 Types of superconductors

The most basic phenomenon associated with superconductivity is zero resistance below a critical temperature T_c. According to the BCS theory [6], this state is possible due to an attractive interaction between electrons which is mediated by the lattice (phonons). Due to the aforesaid interaction, electrons tend to pair into bosons (Cooper pairs) which in turn allows them to condense into a single energy state. This process results in an energy gap, Δ, around the Fermi level. This energy gap depends on temperature and relates to the critical temperature by $\Delta = 3.52 k_b T_c \sqrt{1 - T/T_c}$ where k_b is the Boltzmann constant.

Superconductors can be classified into two classes. In type-I superconductors a magnetic field is expelled by creation of superconducting currents that balance it out. This phenomenon is called "Meissner effect". In type-II superconductors things are more complicated. In a magnetic field lower than a critical value H_{c_1} the Meissner effect holds just like in type-I superconductors; however an intermediate state occurs when $H_{c_1} < H < H_{c_2}$. In this state the magnetic field pierces the superconductor in cylindrical cores in which superconductivity is suppressed. The magnetic flux penetrating the superconductor induces a supercurrent that flows around this normal core in order to prevent the magnetic field from further invading the superconductor, hence the term commonly used to describe these beings: 'vortex'. When the external magnetic field exceeds the second critical field, H_{c_2} superconductivity is destroyed altogether.

Figure 1.2 summarizes the different phases of both types of superconductors.

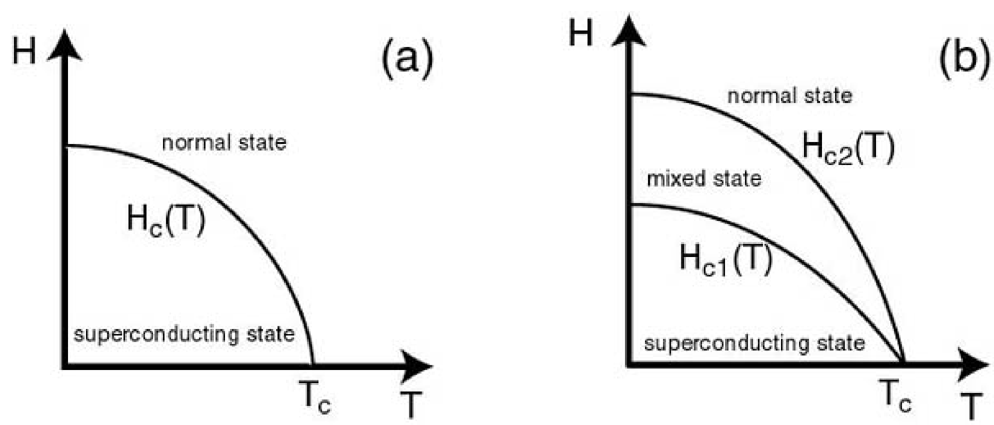

Figure 1.2: *Phase diagrams of (a) Type-I superconductors and (b) type-II superconductors*

Vortices in a superconductor are subjected to many different forces acting upon them, one of them being the pinning force. Defects in the superconductor lead to a local potential well which exerts force on the vortex causing it to stay in a pinning site. In order to move a vortex one would have to exert a force on it greater than the pinning force.

Another force acting on a vortex is the Magnus force which exists when a current flows in the mixed state of a type-II superconductor. This force is given by $\vec{F}_M = \rho_s \vec{v} \times \vec{\kappa}$ where ρ_s is the superconducting condensate density, $\vec{v}$ is the velocity of the vortex relative to the condensate in the direction of the current and $\vec{\kappa}$ is the circulation vector. This force acts in a direction perpendicular to the superconducting current.

If this force is greater than the pinning force, the vortex will move in a direction perpendicular to the current. When the vortex moves with a velocity v_L it causes a time dependence of the magnetic flux and thereby induces an electric field of magnitude $\vec{E} = \vec{B} \times \frac{\vec{v_L}}{c}$ which in turn causes a voltage drop along the direction of the electric field. A voltage drop across a superconductor which carries current implies a resistance $R = V/I$ which causes dissipation of power in the superconductor.

1.2.2 Phase slips

In the framework of the Ginzburg-Landau theory [7] a complex order parameter $\Psi = \sqrt{\rho_s} e^{i\phi}$, where ρ_s is the superconducting condensate density and ϕ is the phase, is introduced in order to describe superconductivity. Since the order parameter has to be single-valued, when traveling along any closed path the total phase of the path has to be $\Delta\phi = 2\pi n$, n being an integer. This phase shift depends on the total magnetic flux through the closed path. Hence the magnetic flux quantum that can penetrate a superconductor is $\Phi_0 = \frac{h}{2e}$. In addition, we recall the Josephson relation that states that a phase change in time induces a voltage drop

$$V = \frac{\Phi_0}{2\pi}\dot{\phi} \tag{1.4}$$

This result means that the creation and annihilation of a vortex induces a voltage drop.

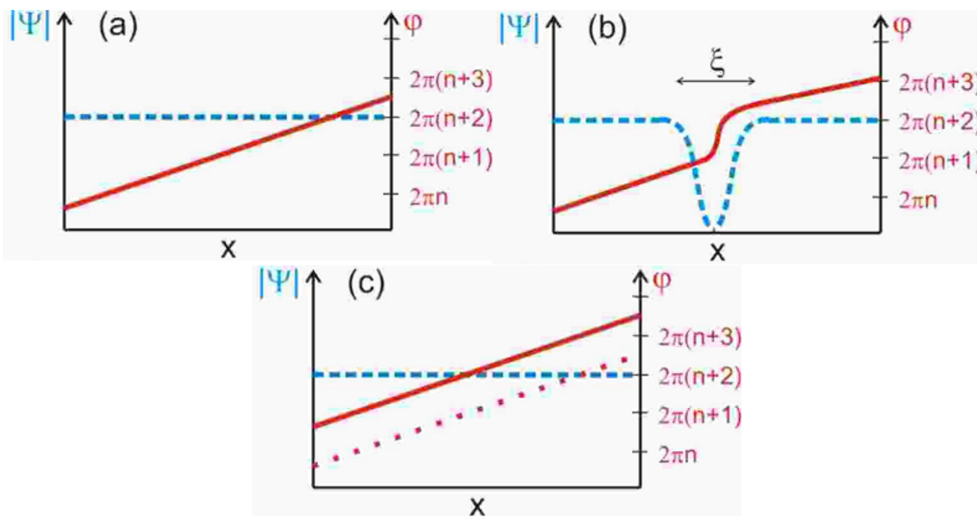

Figure 1.3: *Schematics of the phase slip process, taken from [8]: the GL order parameter's modolus and phase (a) before (b) during (c) after the process of phase slip. Note that the phase is shifted from its initial value when the process is over, implying a change in time and therefore a voltage drop around the core.*

In the case of one dimensional superconductors, where the width of a wire

d is smaller than the superconducting coherence length ξ superconductivity is inherently unstable. In this case thermal fluctuations may cause the modulus of the order parameter to vanish momentarily and thus allow the phase of the superconductor to slip by $2\pi n$. When superconductivity is restored the phase continuity is restored and the phase takes take a new value, as depicted in figure 1.3. Once again, using the Josephson relation we can conclude that a momentary voltage drop will appear along the superconductor.

If $d > \xi$ a voltage can also appear in the presence of superconductivity. In this case the forces acting on vortex-antivortex pairs break them and cause them to move in opposite directions, which in turn induces a voltage.

1.2.3 The Nernst effect

In normal conductors a combination between a temperature gradient and a magnetic field may cause an electric field and a voltage drop perpendicular to both fields. The size of this effect, called the Nernst effect, is given by:

$$|N| = \frac{E_y}{\frac{dT}{dx} B_z} \tag{1.5}$$

where $|N|$ is the Nernst coefficient, E_y is the y component of the electric field, B_z is the z component of the magnetic field and $\frac{dT}{dx}$ is the temperature gradient in the x direction. This effect typically yields a very small voltage drop of the order of a few nanovolts (nV) when $B_z = 1T$ and $\Delta T = 1K$.

In type-II superconductors a temperature gradient may cause vortex movement in a direction parallel to it and perpendicular to the external

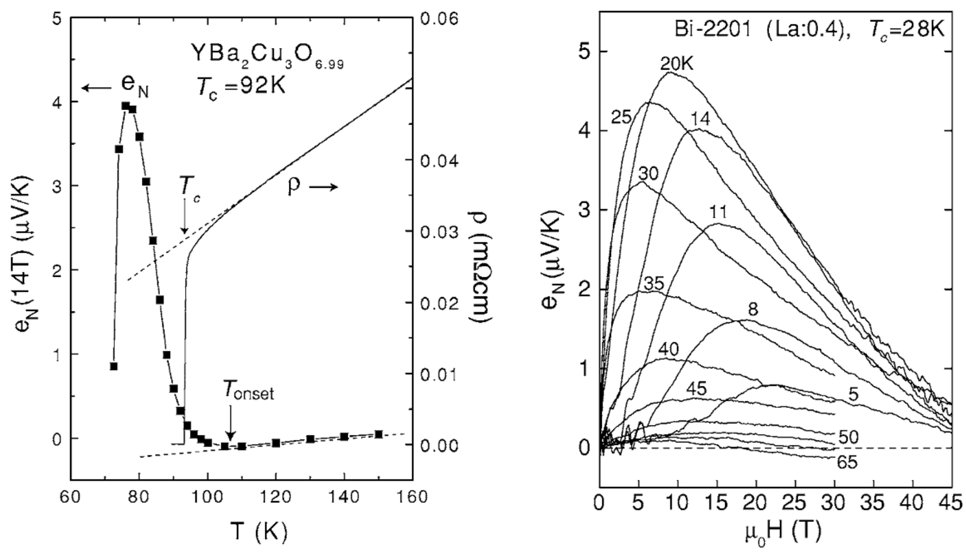

Figure 1.4: *left: (solid line) resistivity ρ of a YBCO sample vs. temperature. (line with squares) the nernst signal (notated here with e_N) measured at 14 Tesla in the same sample. right: Nernst signal vs. magnetic field in a Bi-2201 sample at different temperatures. Due to vortex-antivortex symmetry the graph is antisymmetric with magnetic field. Figures are taken from Ref. [9].*

magnetic field, thereby inducing an electrical field. This is known as the Superconducting Nernst effect. In this effect equation 1.5 does not apply. Instead the nernst coefficient takes a special form which is thoroughly described in [9]. In general the Nernst signal increases in low fields until the critical field is reached, followed by a decrease in the signal. When $H \to H_{c2}^{-}$, the nernst signal behaves linearly with the sample's magnetization. Figure 1.4a depicts the Nernst signal in YBCO versus temperature, and Fig. 1.4b depicts the Nernst signal in Bi-2201 versus magnetic field. As can be seen, both curves show an extremum of the Nernst signal, though the cause for these extrema are somewhat different. The extremum in Fig. 1.4a is present since superconducting fluctuations are most abundant at the border between the superconducting and normal states. The extremum in Fig. 1.4b is due to the destruction of superconductivity. When trying to quantify the effect's behavior in magnetic field it seems useful to address the coordinates V_{max}, H_{max} of the peak. We will use these parameters in another section when describing our results. From Fig. 1.4 it is visible that H_{max} decreases with the increase of temperature and that V_{max} has a maximum at some temperature below the material's T_c.

One of the most important differences between normal and superconducting Nernst effect is that in type-II superconductors the Nernst signal can reach a very large value of a few microvolts, which makes it easier to measure experimentally.

1.2.4 Vortex ratchet effect

If a vortex is subjected to a time varying force which averages to zero, i.e. AC force, it is naïvely expected to create a voltage drop which follows the same time dependence and therefore average to zero as well. If, however, the pinning potential is asymmetric this would leads to a preferred direction of movement for the vortices. If an AC bias is applied to such a system, this will cause a net movement of the vortices and a ”rectification” leading to a DC voltage in what is called the vortex ratchet effect [10]. A schematic picture of such a system is given in Fig. 1.5.

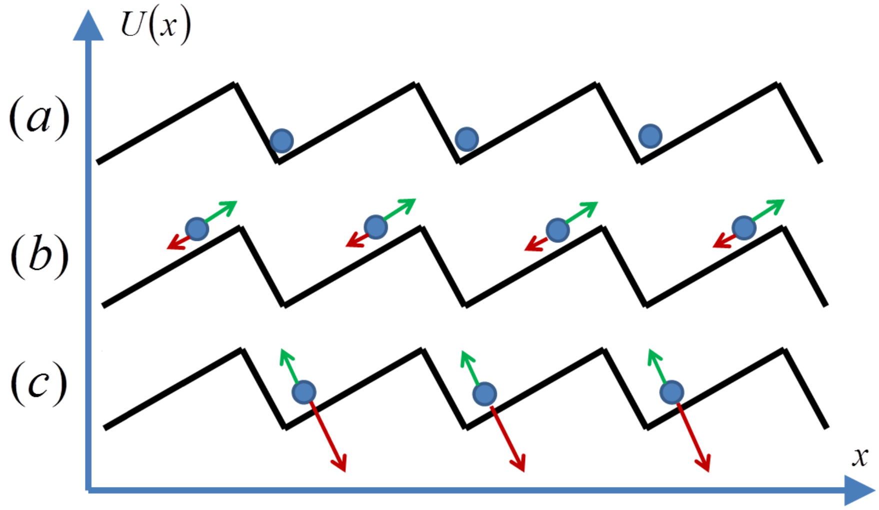

Figure 1.5: *a schematic description of the ratchet effect: (a) particles (i.e. vortices) are located in asymmetric potential wells that are spread along the sample. (b) an external force (green arrows) moves the particles outside the well and into the adjacent well, as the pinning force (red arrows) is weaker than the external force. (c) in the other direction the pinning force is stronger than the external force and so the particles stay in their pinning sites.*

Fig. 1.6 shows the behavior of this effect when applying AC currents of different amplitude to such an array. In this case the pinning sites were intentionally fabricated in the asymmetric shape of triangles. These pinning sites make the vortices favor the upward direction over the downward. One

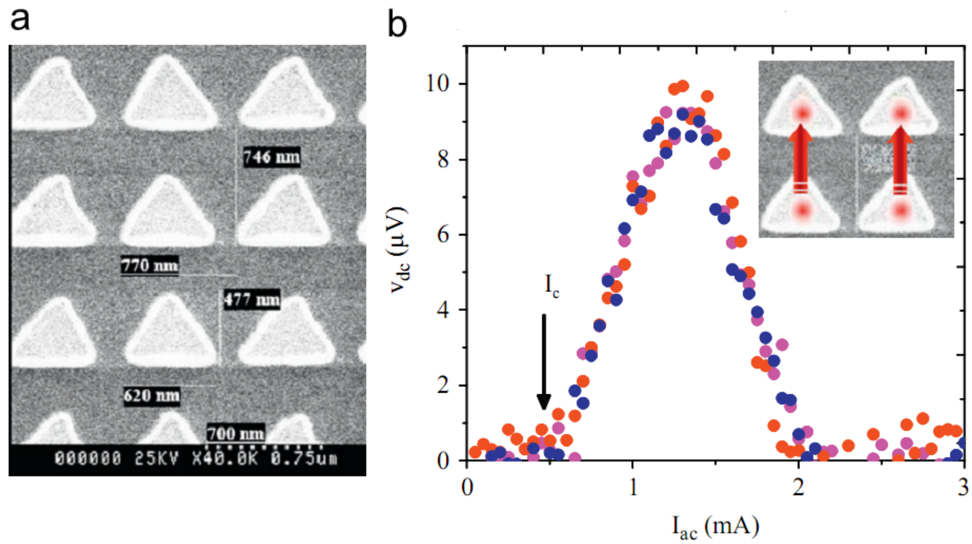

Figure 1.6: *(a) SEM picture of an array of asymmetric Ni triangles acting as pinning sites in a 100nm thick film of Nb. (b) DC voltage measured in the y direction as a function of the AC current amplitude, driven in the x direction through the array shown in (a). Different curves show different frequencies of* $\omega = 10kHz$, $\omega = 1kHz$ *and* $\omega = 0.5kHz$ *for magenta, blue and red circles, respectively. Taken from reference [10].*

noticeable feature in this figure is a threshold current for the onset of the effect, easily explained as the minimum force required to pull a vortex away from a pinning site. The observed upper cutoff of the effect happens when the amplitude of the force is high enough so the pinning force in any direction is negligible compared to it, causing the vortices to move from site to site in both directions. The intermediate peak is where the difference between the vortices' forward speed and backwards speed is maximal.

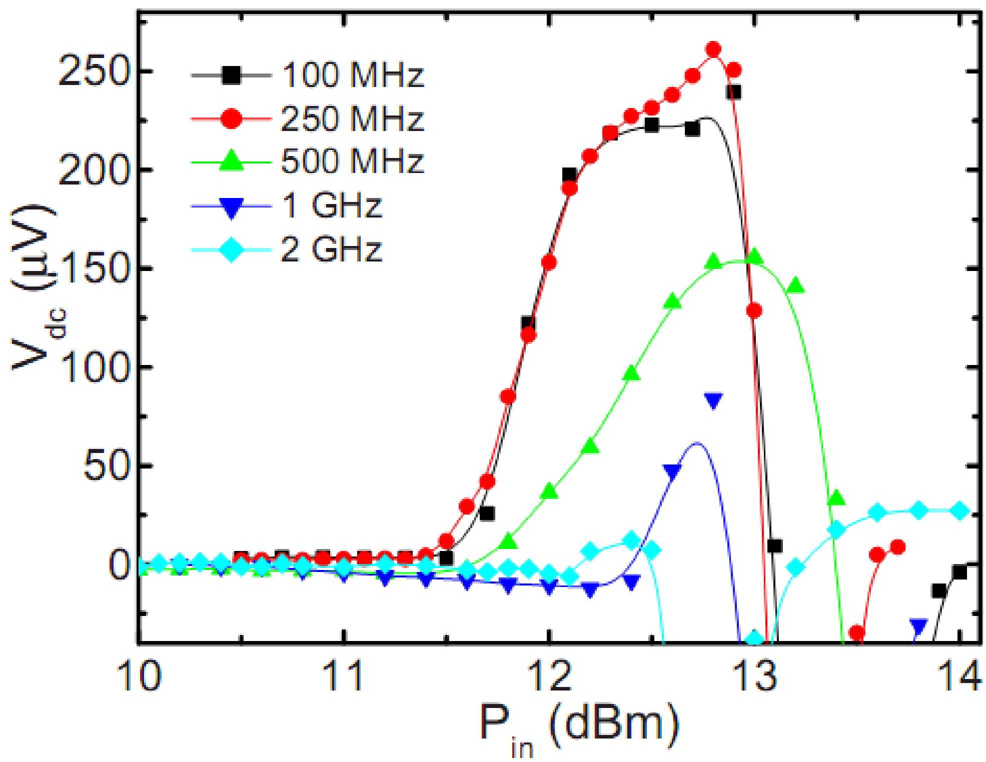

Figure 1.7: *Rectified voltage as a function of power supplied (not proportional to the absorbed power in different frequencies due to RF considerations) for different frequencies. Taken from reference [11].*

In Fig. 1.7 the effect is portrayed for several frequencies. It seems that the effect is suppressed at high frequencies . This can be attributed to the fact that the direction of the force is reversed before the vortex reaches the next pinning site.

1.3 Superconductor-insulator transition

It was believed in the past that when superconductivity is destroyed by an external parameter, e.g. a magnetic field, the resultant material will possess metallic properties. However in the past three decades a small class of superconducting materials exhibited insulating properties when their superconductivity was destroyed [12]. This transition between a superconducting and an insulating ground state is known as the superconductor-insulator transition (SIT). This work focuses on the case where the parameter that induces this transition is the level of disorder in the system.

1.3.1 Homogeneous versus granular SIT

As noted above, disorder can be viewed as the introduction of a random potential to an ordered system. Let l_d be the characteristic length at which the disorder's inhomogeneity changes substantially and let l_a be the characteristic atomic length scale of the system. In the case of $l_d \sim l_a$ the disorder is considered uniform and the other limiting case of $l_a < l_d$ is called "granular" in the sense that materials in this limit may hold superconductivity in islands in which disorder is relatively low.

The SIT in these two limits has been studied experimentally. Figure 1.8 depicts experiments on thin granular and homogeneous Pb films [13]. In these graphs resistance as a function of temperature curves are presented, each curve corresponding to a different thickness, where the top lines are the thinnest and the bottom lines are the thickest. The thickness of the films in this case is interpreted as a measure of disorder, where thin films are more disordered.

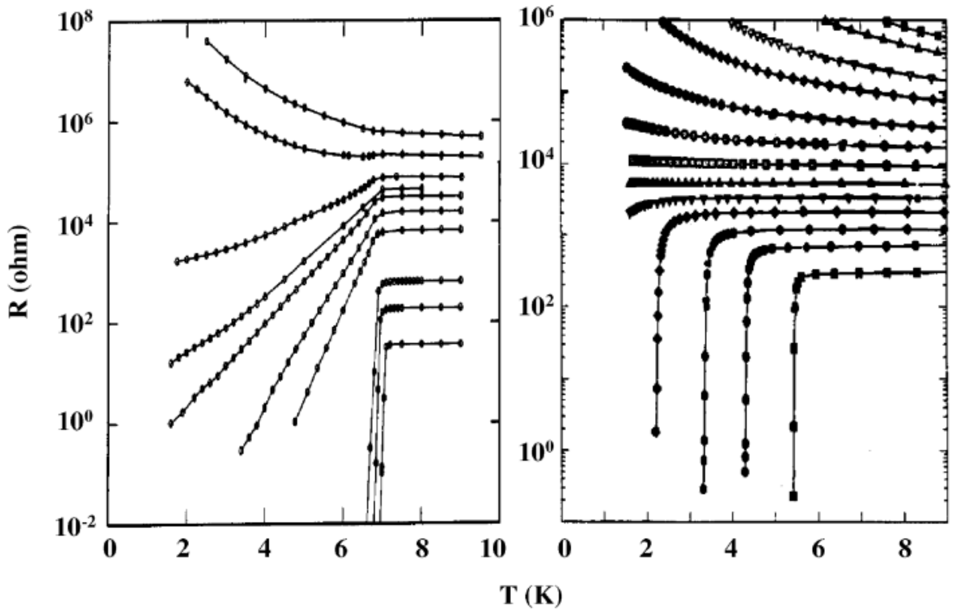

Figure 1.8: *RT curves of Pb thin films at different thicknesses, fabricated (left) in granular form and (right) in a uniform geometry. Taken from reference [13].*

There are several noticeable differences between the two cases. For one, the point at which the slope of the curve changes, presumably by the onset of superconductivity, is fairly constant in the granular case and equals the bulk T_c of Pb, $7.2K$. In the homogeneous case this point changes considerably, approaching the bulk T_c of Pb upon lowering of disorder. Another significant difference is the existence of an intermediate state in the granular case, between insulator and superconductor, which is characterized by a gradual descent of the resistance. This state is seemingly absent in the homogeneous case.

A popular explanation for the difference in results between the two geometries is that in the granular case each grain is a bulk superconductor and that the superconducting grains are coupled via Josephson junctions, and in the homogeneous case superconductivity is absent throughout the sample until a critical disorder value is crossed.

Relating this explanation to the GL order parameter, one can say that in the homogeneous case the modulus of the order parameter equals zero in the sample while in the granular case the modulus is not zero, but rather the phase fluctuations between grains prohibits coherence through the sample. These phase fluctuations get smaller with decreasing disorder, thus making the sample show an RT curve closer to that of the bulk superconductor.

1.3.2 Third kind of SIT

Though the two aforesaid situations may be relevant to many of the experimental systems, another class of materials shows peculiar SIT phenomena. Examples of such materials are films of Indium Oxide with thickness $d > 20nm$, thin films of Titanium Nitride with thickness $d \approx 5nm$ and ultra thin films of Beryllium that consist of several atomic layers. These films are structurally amorphous but show signs for strong inhomogeneity in the superconducting properties. We shall now present a few of those phenomena.

Scale dependent SIT

When a series of InO films with common width and varying lengths were measured as a function of disorder they showed interesting behavior [14]. As can be seen in figure 1.9, immediately after fabrication all of the films showed insulating behavior. However, after evenly lowering the disorder in all of the samples the shorter ones exhibited superconductivity while the longer ones remained insulating. These results imply that the samples are inhomogeneous even in the scale of a few microns, and that a percolation of the superconducting regions occurs as a function of disorder.

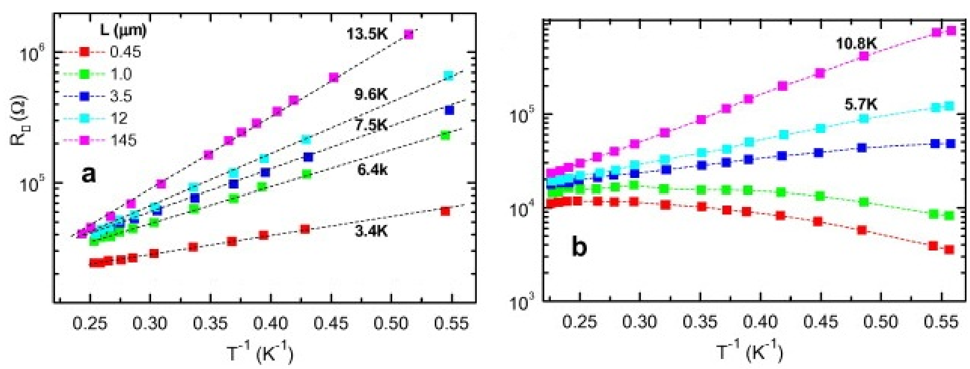

Figure 1.9: *R(T) lines of InO samples of common width and disorder. Each line represent a sample of different length. The left graph is at a higher level of disorder than the right one. Taken from reference [14].*

Giant magnetoresistance peak

In reference [15] the magnetoresistance of InO films was studied. As seen in figure 1.10, when a magnetic field is applied, the resistance raises until it reaches a maximum value much higher than the normal state value and then decreases to the normal state resistance at very high field. The experiment was conducted in two different orientations of the magnetic field, both of which resulted in similar results. Though no satisfactory explanation has been given for this phenomenon - a common explanation is the following:.

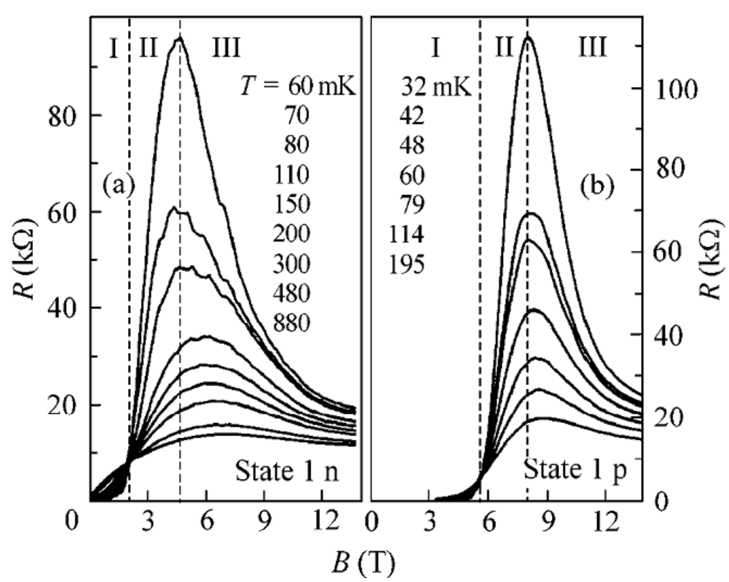

Figure 1.10: *Isotherms R(B) of InO films for (a) perpendicular and (b) parallel magnetic field. Taken from ref. [15]*

Assuming that electronic granularity exists in the material, magnetic field gradually decreases the size of superconducting islands which causes an interplay between cooper pairs hopping and normal conduction [16]. In low and high magnetic fields the conduction is mainly superconducting and normal, respectively. Near the peak tunneling between superconducting islands is difficult, and so is conduction around the islands, in narrow bands of normal material. In this state both superconducting and normal conductivities are low, which gives rise to the peak in resistance.

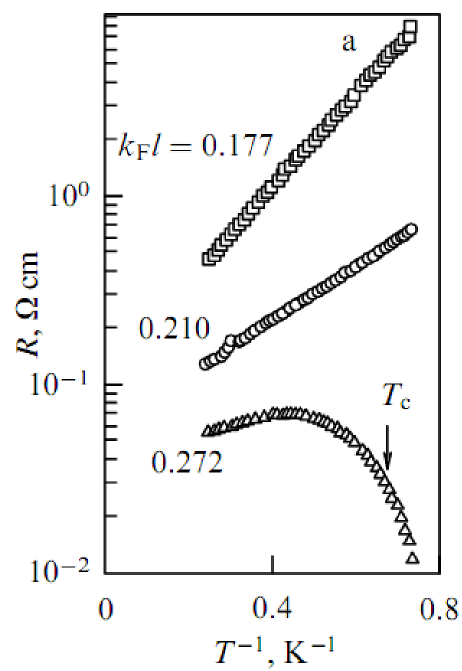

Figure 1.11: *Temperature dependence of the resistance of an amorphous InO film 200nm thick for three levels of disorder. Taken from ref. [18]*

Arrhenius behavior

On the insulator side these materials are expected to show characteristics of an Anderson insulator, and therefore its conductance is expected to show temperature dependence of variable range hopping, as described in Eq. 1.2, or in some cases it should follow Eq. 1.3 as explained in [17]. However, results on InO [18] depicted in figure 1.11 show a resistance that follows a simple Arrhenius behavior $R \propto e^{\frac{T_0}{T}}$ in contradiction to the fractional exponent suggested in equation 1.2.

Such behavior is typical of a system which is characterized by a single energy barrier of a well-defined value, and not by a wide distribution of energies. It is unclear why such a behavior appears. One possible explanation is that the existence of cooper pairs in the insulating state allows their binding energy to be the characteristic energy level of this system.

Gap above T_c

The density of states in TiN thin films has been studied close to the SIT [19] by means of STM measurements. An example for such measurement is shown in figure 1.12. It is seen that an energy gap is visible even at temperatures higher than T_c. Above T_c the gap lacks the coherence peaks that are characteristic of a superconductive gap.

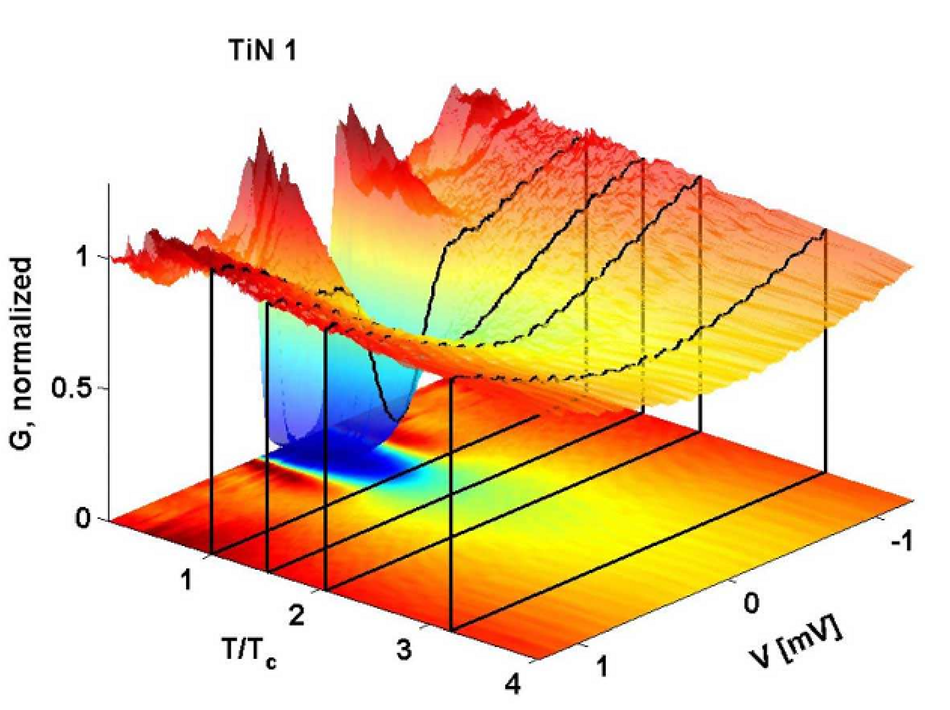

Figure 1.12: *DOS of a thin TiN layer showing a gap above T_c. temperature normalized to T_c indicates clearly that a gap exists above $T/Tc = 1$. Taken from ref. [19]*

All the listed unexplained phenomena that appear in this class of materials points to a need for further experiments in order to shed light and assist in theoretical understanding. In our work we explored 1D wires of disordered InO in order to try to help in future understanding of this subject.

Chapter 2

Research goal

The SIT has proven to be a fertile ground for research in the past three decades. The absence of a complete explanation for a wide collection of supposedly related phenomena only increases the interest in further experiments.

In this work we conducted a variety of experiments on disordered amorphous InO nanowires in an attempt to add to the accumulating knowledge regarding this phenomenon. The main tools of this research were fabrication of different nanowire geometries, measurements in low temperatures and the use of a magnetic field.

Analyzing our results may aid to the future understanding of the SIT in disordered systems.

Chapter 3

Experimental

3.1 Indium Oxide

When a high purity In_2O_3 is deposited on a SiO_2 substrate using e-beam evaporation in vacuum, an amorphous InO_x film is formed with a certain Oxygen deficit $q = 1.5 - x$ [18]. This Oxygen deficit depends on the Oxygen pressure in the chamber in the deposition process. Small changes to this deficit, either increasing or decreasing it, can be made after the deposition by thermal annealing at low temperatures of $T < 100°C$. Annealing which takes place in vacuum increases q by freeing Oxygen atoms and this decreases the material's resistivity, and annealing in air, where oxygen is abundant, decreases q and increases the material's resistivity. This process is continuous in time, so longer annealing times correspond to larger changes in q, however the rate of change decreases rapidly, making long annealing times inefficient and possibly futile.

These Oxygen vacancies act as donors and change the carrier concentration n in the film. These charges can either be localized by the random potential of the amorphous material or, if n is larger than some critical value n_c, they can be delocalized. When lowering the temperature below the material's T_c the delocalized electrons can pair and turn the material into a superconductor.

3.2 Sample preparation

The samples in this work were fabricated on a Si wafer with a thick layer of SiO_2 on its surface. In order to fabricate large electric leads (about $2\mu m$ resolution), a photomask was designed and used in a photolithography process. The leads were composed of a layer of Gold $15nm$ thick with an underlayer of Chromium $5nm$ thick to allow the adhesion of gold. Finer (down to $10nm$ resolution) features were fabricated using e-beam lithography with a CABL-9000 scanning electron microscope with a lithography mode to make the nanowire.

The InO e-beam deposition was conducted in pressures of Oxygen that varied from sample to sample in the range of $60 - 80\mu Torr$, and always at a deposition rate of 0.9 $\mathring{A}$/second. In order to reduce the disorder between two consecutive stages of the experiment the samples were annealed in vacuum at $80°C$ without breaking the vacuum from measurements, so the possibility that exposure to atmosphere affects our results is avoided.

The nanowires were fabricated in three different geometries: $0.8\mu m \times 50nm$, $6.33\mu m \times 50nm$ and $5.8\mu m \times 100nm$. The thickness of the deposited material was always $30nm$. The shortest nanowires ($l = 800nm$) were connected to four InO leads to allow four-terminal measurements and the longer ones ($l = 6.33, 5.8\mu m$) were deposited directly on the gold leads. A large scale photo of the sample is shown in Fig. 3.1 and a close-up on a short nanowire with four probes is shown in Fig. 3.2.

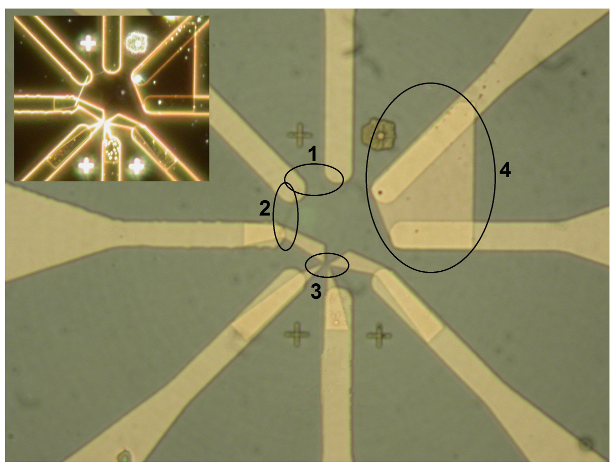

Figure 3.1: *A picture of the studied samples: 1 + 2 (hardly visible): The longer nanowires, about* $5-6\mu m$*, connected to two probes. 3: A short nanowire with four probes. 4: A short between leads, used as a heater. Inset: Dark field photo of the same sample, where the longer nanowires are more easily observed.*

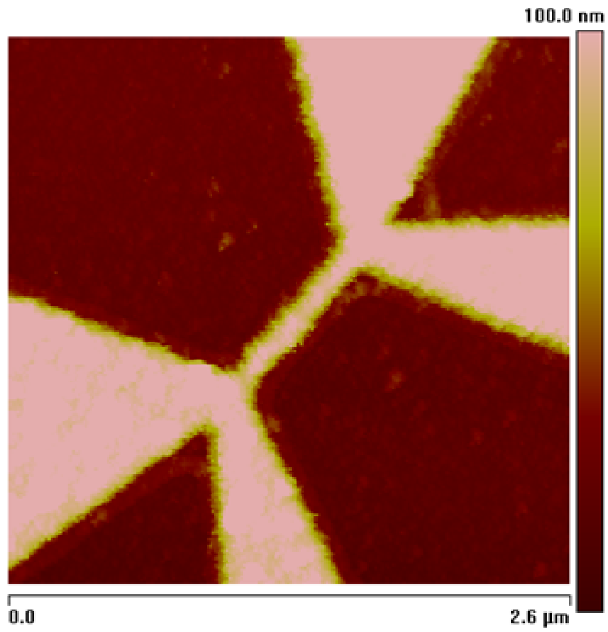

Figure 3.2: *An AFM image of a* 800nm *long and* 60nm *wide nanowire, showing the four probes used for resistance measurements.*

3.3 Measurements

The measurements in this work were conducted in a liquid Helium dewar with a built-in $6T$ superconducting magnet. After the sample was fabricated, it was mounted on a measurement probe with a built-in ^3He system capable of base temperature of $T_{min} < 300mK$. Data was obtained using home made LabView programs.

3.3.1 Resistance measurements

Resistance measurements were taken both by DC measurements and low frequency AC measurements with a lock-in amplifier. The current was kept around 0.1-10nA, in order to avoid Joule heating of the sample. In the normal state we always made sure that the current is low enough to show ohmic behavior. When using the the lock-in amplifier its frequency was set to a value which minimizes noise, in the $2 - 15Hz$ regime. The signal to noise ratio in the measurements was typically above $S/N = 100$.

DC measurements were taken with Keithley 6001 current source and a 2182A nanovoltmeter, and AC measurements were taken with a DSP 7265 or an SR-830 lock-ins with internal oscillators.

3.3.2 Voltage measurements

DC voltage measurements were conducted by connecting two probes to either a Keithley 2000 voltmeter or alternatively a Keithley 2182A nanovoltmeter for better accuracy.

3.3.3 Resistance/Voltage vs. Temperature (RT/VT)

The sample was heated using Joule heating of a resistor embedded into the sample holder to a temperature of about 7K and then sweeped down to base temperature measuring resistance or DC voltage. Some of the measurements were performed in the presence of an external magnetic field with the aid of the superconducting magnet.

3.3.4 Resistance/Voltage vs. Magnetic field (RH/VH)

The sample was kept at a constant temperature in the range of 300mK-7K by Joule heating the sample holder after it was brought to base temperature, and R or V were measured while sweeping the magnetic field at different ranges and rates.

3.3.5 Measurements in a temperature gradient

As will be explained later it was necessary to take measurements while a temperature gradient was imposed on the system. In order to do so two of the leads where shorted by a Cr/Au pad using an additional lithography process to allow Joule heating close to one side of the nanowire. The other end of the nanowire is expected to stay cooler both because it is farther away from the heat source and because the sample holder is coupled to a cold reservoir (^3He bath). A picture showing the heater is given in Fig. 3.1.

3.3.6 RF measurements

As will be explained later it was necessary to take measurements in the presence of radiation in the vicinity of the sample. In order to create this radiation a Rhode&Schwarz SMG signal generator was used, which has a frequency range of $100KHz - 1GHz$ and amplitude up to $16dBm (= 40mW)$.

The radiation was pushed in through a gold lead located at a distance of about $20\mu m$ from the nanowire. At the same time an HP 8560A spectrum analyzer was connected to another loose gold lead to track the radiation in the measurement chamber.

This technique is problematic as we have no good indication about the power that's picked up by the sample, and so it is used mainly as a qualitative mean and not as a quantitative measure.

Chapter 4

Results

In this work we conducted experiments on a variety of samples that showed reproducible phenomena. Table 4.1 lists the samples that we report in this work and their sizes.

Name	Width(nm)	Length(μm)	Thickness (nm)
NW7	50	0.8	30
NW8	50	0.8	30
NW11	50	0.8	30
NW12	100	5.8	30
NW13	50	6.3	30
NW14	100	5.8	30

Table 4.1: *Sample geometries*

We saw similar behavior in all 14 nanowires studied so far, and these results are hereby reported.

4.1 Resistance of nanowires

The nanowires in our experiments showed room-temperature resistances in the range of $10K\Omega$s up to one $M\Omega$, where nanowires evaporated with high Oxygen pressure (corresponding to higher disorder) showed resistances much higher than the ones fabricated with low Oxygen pressure. The resistance of the nanowires did not follow the expected behavior of $R = \rho l/A$. For example NW12 and NW13 were fabricated in the same evaporation and therefore are expected to have the same level of disorder and the same sheet resistance, however the former, which is the narrower one, had sheet resistance of $R_{sq} = 5371\Omega/sq$ and the latter had $R_{sq} = 1379\Omega/sq$.

When the samples were cooled to low temperatures three different regimes could be identified:

"Strong disorder" the samples' resistance increases rapidly with lowering temperature, as expected from an insulator.

"intermediate disorder" below "T_c" the resistance was raised to a value higher than its normal state resistance and saturated below a certain temperature, reaching a resistance plateau.

"Weak disorder" below "T_c" the resistance decreased to a value lower than its normal state resistance and saturated at a plateau.

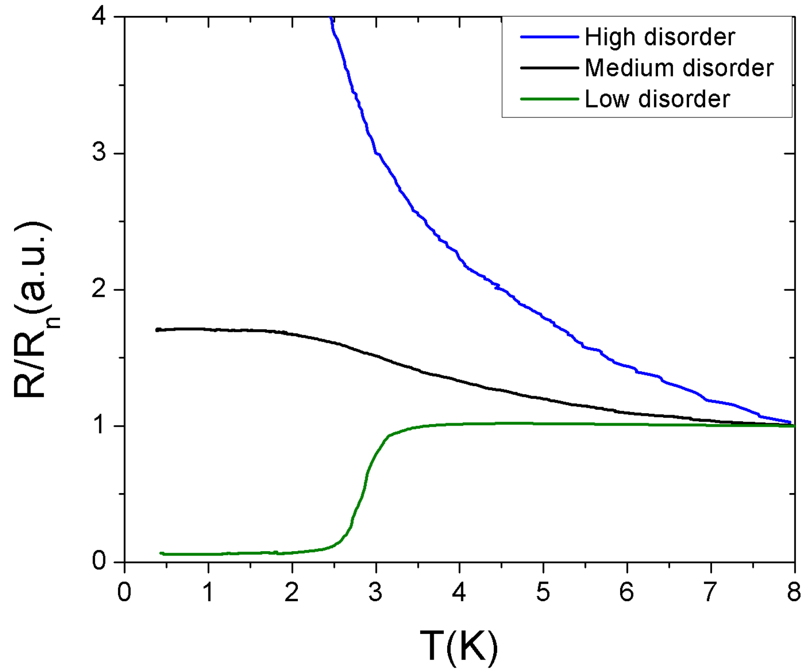

Figure 4.1: *General behavior of the nanowires in high, medium and low degrees of disorder. Note that the resistance does not drop to zero even in the weak disorder regime.*

We note that the terms of strong, intermediate and weak disorder are used in other works that involve weak localization, Anderson localization and other phenomena. In our framework they are used to define levels of disorder that correspond to the behavior of the samples.

Figure 4.1 demonstrates the three different behaviors. Note that none of the nanowires showed entirely zero resistance, even after extremely long annealing times. This is counterintuitive since in a work by D. Shahar *et al.* [20] the state of correlated superconductivity was achieved in InO nanowires. One possibility though is that their fabrication process enabled them to reach levels of disorder much lower than those we could reach in our samples. In the discussion we will propose that this resistance is of an external source which did not exist in this experiment.

Further measurements have been conducted to try and reveal the cause for the residual resistance at low temperatures, however at this moment it is not well understood. Therefore in this work we will concentrate on the results to be reported in the next section. The current section will not be discussed, and it is planned to be the subject of future projects.

4.2 Voltage along nanowires

4.2.1 Voltage versus temperature

At low temperatures a surprising phenomenon was observed: A voltage appeared to drop spontaneously along the wire below T_c with no external current nor any other bias intently applied to it. This voltage appeared when the wire was at the intermediate or weak disorder regime. The voltage always increased rapidly below T_c and eventually saturated at low temperature as shown in figure 4.2. When reversing the measurement polarity this voltage showed the same curve with negated values and a shift which is negligible and can be attributed to the measurement device's offset. A small amount of voltage also appeared just above T_c

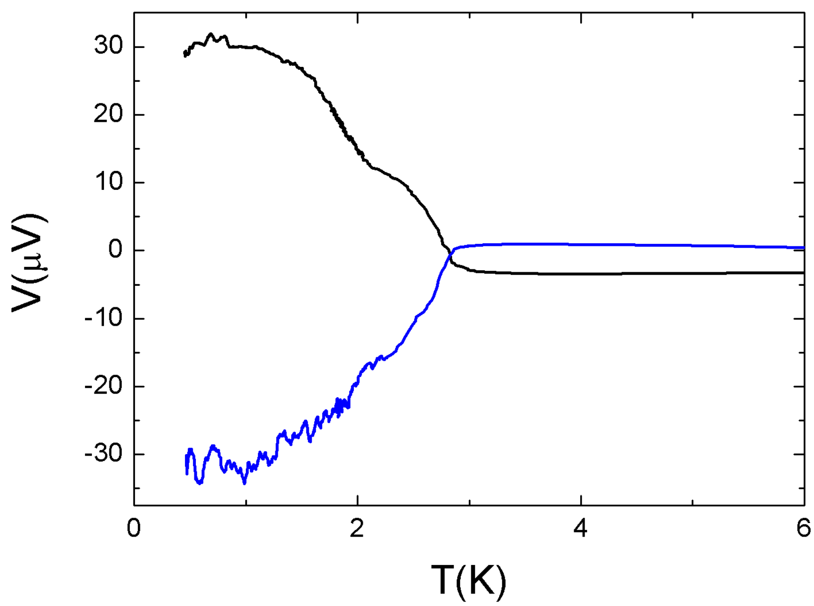

Figure 4.2: *The voltage along NW8 measured with no external bias at two different polarities. The small shift in voltage is due to measurement inaccuracy.*

Fig. 4.3 compares the resistance versus temperature curve and a V_{max} versus temperature curve of the same sample. In this graph the close relation of the resistance and the voltage to superconductivity is shown, as both show a big change in behavior near $T = 3.3K$. It can also be seen that the amplitude has a plateau in low temperatures, perhaps indicating a

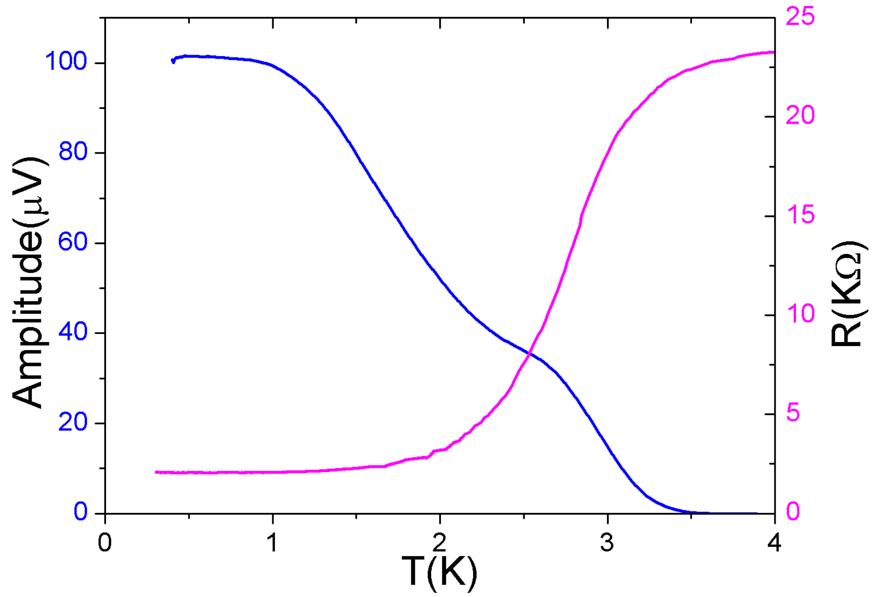

Figure 4.3: *(magenta) resistance of NW11 versus temperature. (blue) amplitude of spontaneous voltage between $H = 0.19T$ and $H = -0.19T$ along NW11 versus temperature. This magnetic field is supposedly H_{max} of this sample.*

mechanism which is independent of temperature in this region.

4.2.2 Voltage versus magnetic field

This spontaneous voltage also showed interesting behavior as a function of magnetic field. As H was increased the voltage was quickly raised in absolute value and then slowly decreased to a value close to its value at zero magnetic field. The decrease was also characterized by a quasi-oscillation that was superimposed on the main curve. This phenomenon showed an antisymmetric behavior upon reversal of the magnetic field ($V(H) = -V(-H)$). An example for one such VH curve is shown in Fig. 4.4.

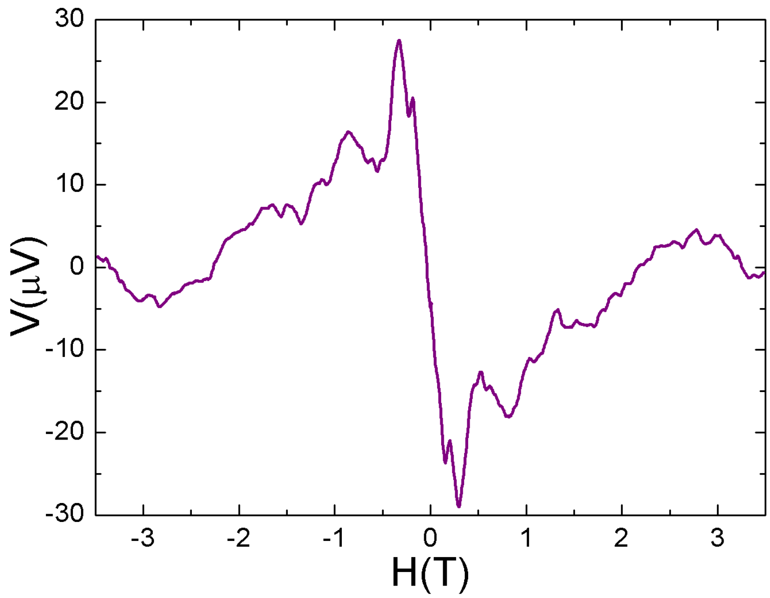

Figure 4.4: *Voltage along NW7 versus magnetic field at base temperature.*

For further discussion of the results we define the field at which the voltage is maximal as H_{max} and the amplitude of the voltage at this point V_{max}, in similarity to the way they were defined in the Nernst signal in chapter 1. Though these parameters are a little difficult to extract in the presence of the superimposed oscillations in our data, they seem to be the most intuitive tool for describing the phenomenon.

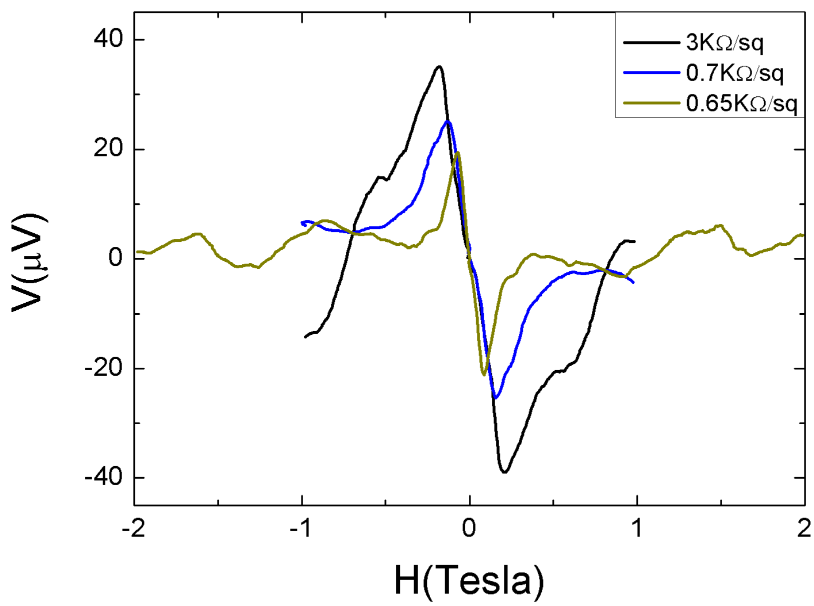

Figure 4.5: *Voltage along NW8 versus magnetic field at* $T = 270mK$ *and at different levels of disorder. The higher the stage the lower the disorder.*

Figure 4.5 shows three VH curves in different degrees of disorder. It is clearly visible that both V_{max} and H_{max} are reduced with lowering the disorder.

Figure 4.6 shows a few VH curves in different temperatures. In this case V_{max} is reduced with increasing temperature until $T = T_c$ is crossed, at which the phenomenon completely disappears. H_{max}, on the other hand, seem not to change at all up to T_c, although it is difficult to determine its exact value.

In an attempt to analyze the behavior the quasi-oscillations which are

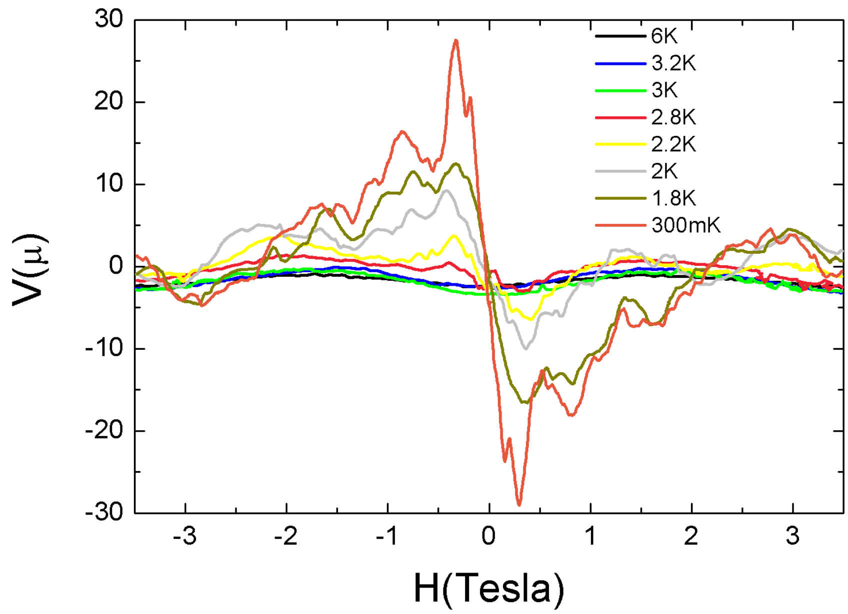

Figure 4.6: *Voltage along NW8 at stage 2 versus magnetic field at different temperatures.*

superimposed over all VH structures fourier transforms (FT) were performed. A characteristic FT is shown in figure 4.7. It is obvious from this graph that quasi-oscillations exist in our measurements, and at least one prominent peak is always observed in the range $0.5T < 1/H < 1.5T$. This magnetic period coincides with a quantum of flux through a square with dimension $37nm < L < 64nm$, which is in the vicinity of the nanowire's width. The rest of the frequency peaks does not reoccur from sample to sample, which may imply that the inhomogeneous random disorder plays an important part

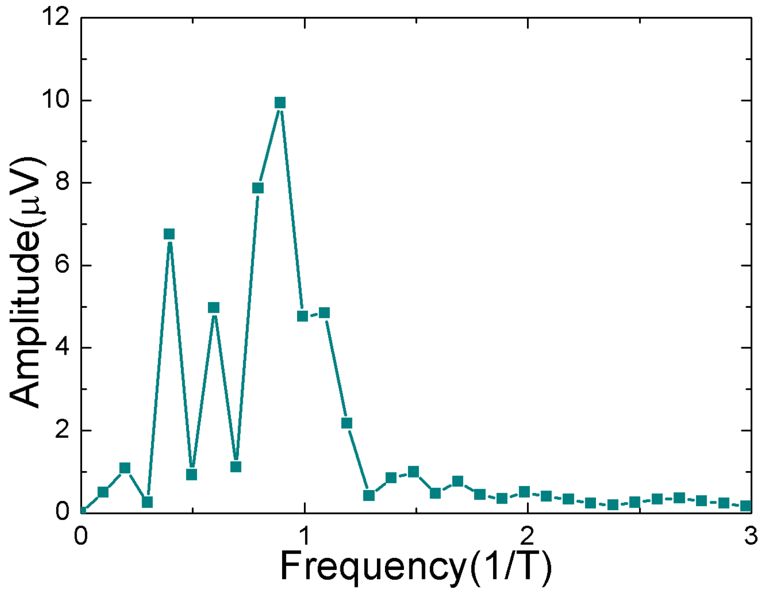

Figure 4.7: *Fourier transform of voltage vs. magnetic field curves of NW12. The FFT is calculated after subtracting a smoothed adjacent-averaging background.*

in determining the sample's response to magnetic fields.

4.2.3 Origins of the voltage

In an attempt to explain the origin of the origin of this voltage we considered the possibility that it is due to a stray capacitance C of the system and charge Q accumulating in it, giving $V = Q/C$. In order to test this option a resistor of resistance R was connected to the system. This resistor should enable discharging of any accumulated charge, which will show an

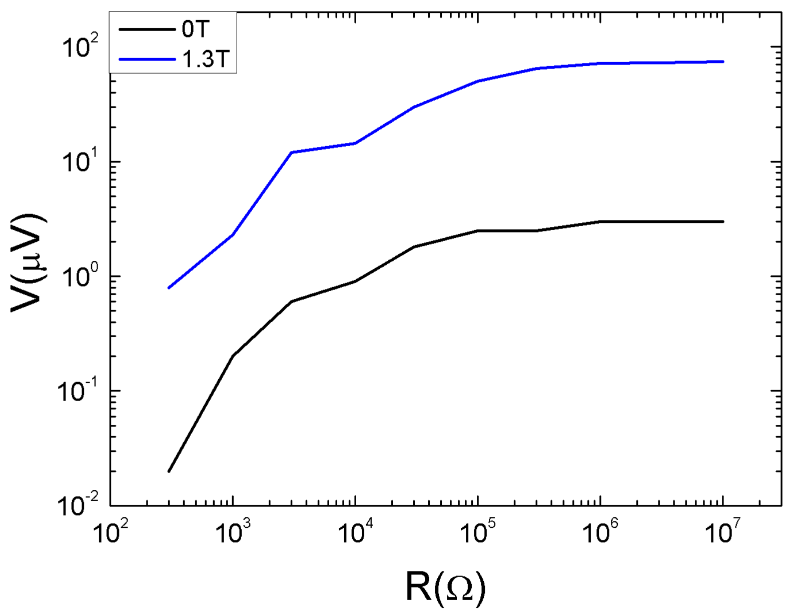

Figure 4.8: *Voltage along NW12 versus the resistor through which it is 'depleted'. Results are at $T = 270mK$ and magnetic field of 1.3T, which is at the first peak.*

exponential decrease of the voltage in time $V = V_0 e^{-\frac{t}{RC}}$. A rough estimate of such capacitance in the case where the leads near the nanowire act as a capacitor gives $A = 1\mu m \times 50nm = 5 \cdot 10^{-14} m^2$ and $d = 1\mu m$ which yields a capacitance of $C = 4.4 \cdot 10^{-21} F$. This is much smaller than the characteristic capacitance of the coaxial wires, which is of the order of picofarads, and therefore negligible. In this case the characteristic time decay of the voltage is $\tau = RC \approx 10^{-6} s$ when using a $1M\Omega$ resistor. This time is far from the available resolution in our framework, which is of the order of milliseconds, and so one would expect a sudden drop to zero voltage when measured versus time in this discharging process.

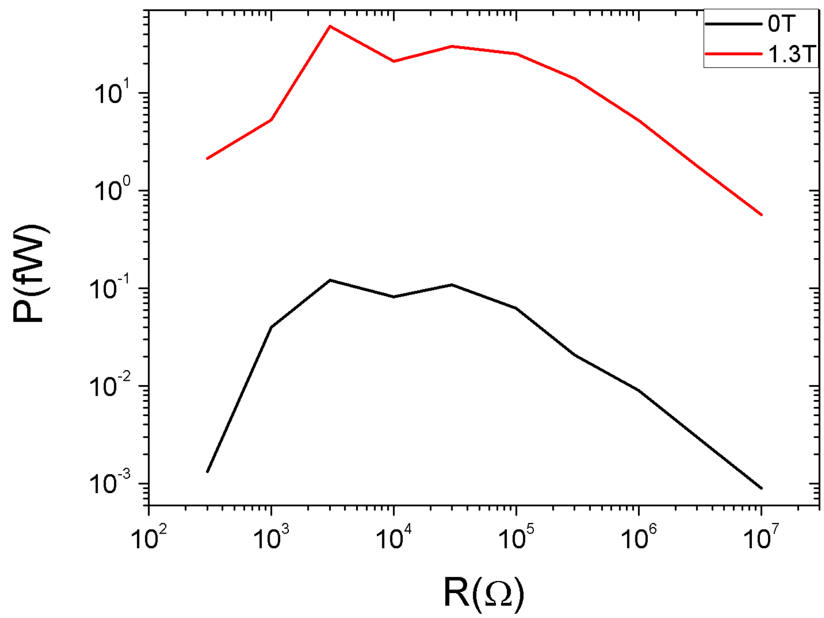

Figure 4.9: *Power on a resistor R connected in series to NW12 at two different magnetic fields and at* $T = 270mK$*. Calculated from the data shown in 4.8 using* $P = V^2/R$

Fig. 4.8 shows the results of one such discharging experiment. Countering the expected results, it shows that instead of dropping to zero the voltage was set to a different value which depended on R. It is also seen that the decrease in voltage starts to be significant when $R < 200k\Omega$, which is of the same order of magnitude as the normal state resistance of this sample, $140k\Omega$.

The existence of this voltage indicates an unexplained sustained imbalance in the system. This imbalance generates power of the order of fW (femto-watts), as can be seen in Fig. 4.9. This is a possible indication of a power source in the system.

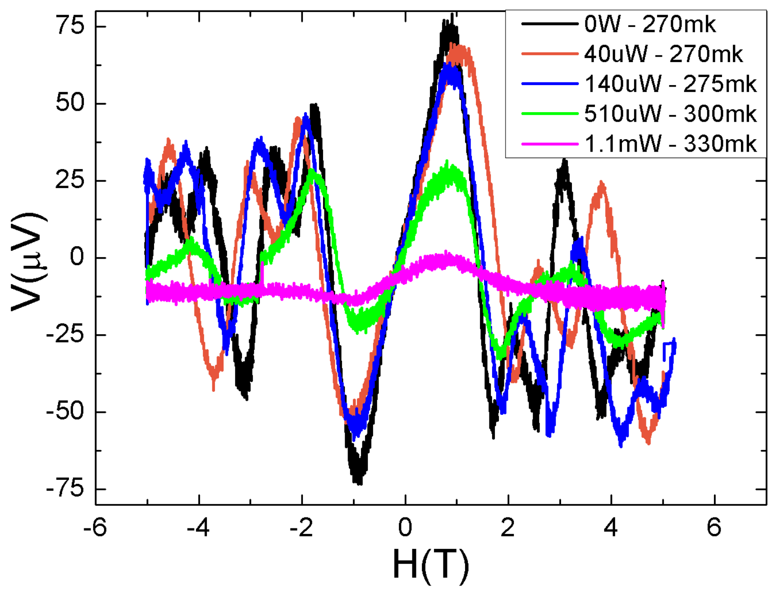

Figure 4.10: *Results of applying the indicated power to a gold wire a few micrometers from the nanowire. Aside from creating a temperature gradient the temperature of the was also changed. The temperature of the sample is stated in the legend.*

We have also considered the possibility that the voltage is caused by Nernst effect by an inherent temperature gradient. In order to test for this possibility a temperature gradient was imposed on the nanowire as described in chapter 3. In the presence of an intentional temperature gradient, which is supposedly larger than a stray one, one would expect to see some change in the Nernst signal. In effect a much larger amplitude is expected to show. The results of an experiment with an intentional temperature gradient are shown in Fig. 4.10. Each curve in this figure corresponds to a different temperature gradient, and it can be seen that the amplitude of this voltage does not increase, but instead decreases until it disappears when the joule heating causes the temperature of the wire to exceed T_c.

Another plausible possibility to explain this voltage drop would be the presence of a leakage of current from the measurement devices. To test this notion an external DC current was driven intentionally through the nanowire and measurements of $V(H)$ were conducted. The results are shown in Fig. 4.11. It is clear that no significant change is observed in the curve. The slight shift in higher magnetic fields is due to the ohmic potential generated and the usual destruction of superconductivity leading to increased resistivity.

After DC effects such as a constant temperature gradient and a DC current were used to probe the behavior of this phenomenon and prove to fail in inducing the spontaneous voltage, an AC approach was used. AC radiation in the frequency range of $0.1 - 1000 MHz$ was generated in the measurement sample. The coupling of the radiation to the transmitting antenna and other environment parameters are unknown. Therefore the used parameter for de-

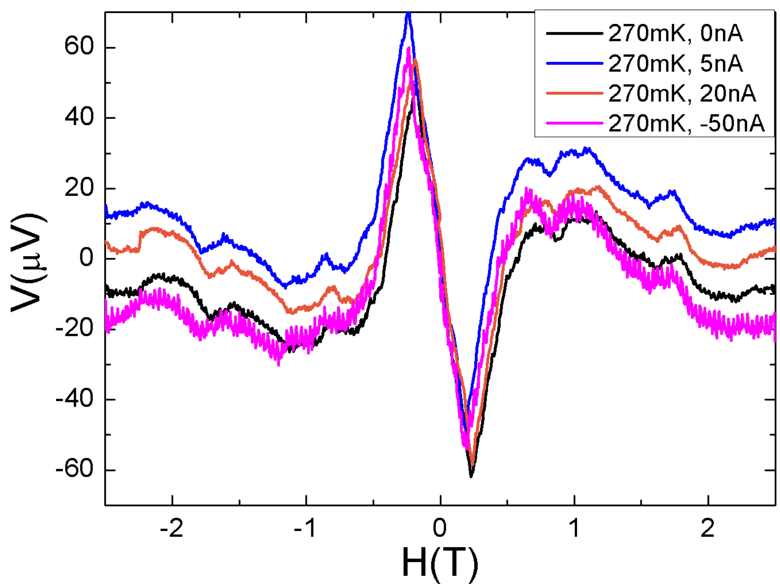

Figure 4.11: *Sweeps of magnetic field when applying different currents through NW11. The measurements were conducted at T=270mK. Results are shifted in the y-axis to (0,0) for easier comparison.*

scribing dependence on this amplitude is the value indicated by the signal generator.

A spectrum analyzer coupled to the chamber revealed that a persistent radiation was imposed in the chamber. This radiation's frequency was about $15.5MHz$ and its amplitude was about $-30dBm(1\mu W)$. This radiation, which is of unknown source, was present at all time. Harmonies of this frequencies were also observed, with smaller amplitudes. Due to this back-

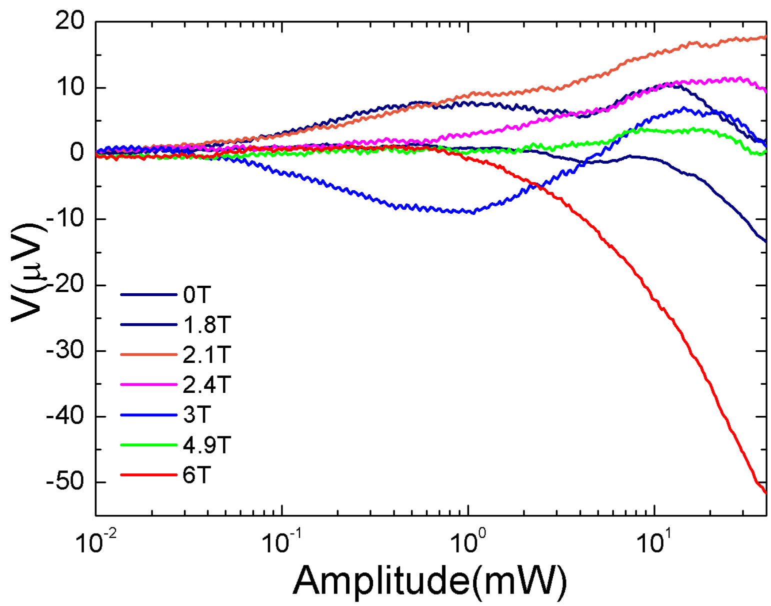

Figure 4.12: *DC voltage along NW14 while radiated with a 100MHz radiation as a function of the radiation's amplitude at different magnetic fields.*

ground radiation, all measurements reported hereafter are in effect the measured value after substraction of a curve measured with no intentional radiation added. All of these AC measurements were conducted at temperature of $270mK$.

In Fig. 4.12 the behavior of the spontaneous voltage is portrayed as a function of AC power. The different curves show different behavior, some monotonous and some non-monotonous, and generally seem not to have recurring features. However the one thing in common is the existence of some

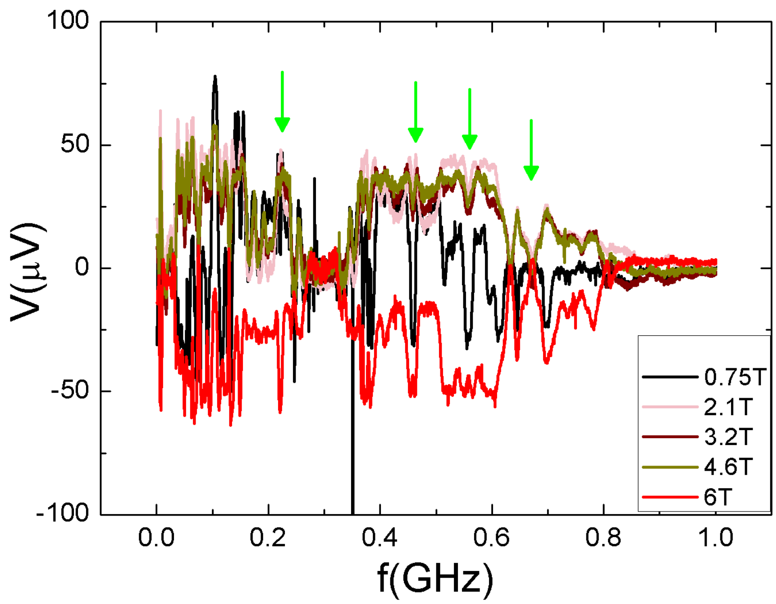

Figure 4.13: *DC voltage along NW14 radiated with a* $10dBm(10mW)$ *radiation as a function of the radiation's frequency at different magnetic fields.*

critical amplitude, A_c, above which the voltage starts to appear. For example, for $H = 1.8, 2.1, 3T$ the critical amplitude is about $A_c \approx 0.04mW$, for $H = 2.4, 6T$ $A_c \approx 0.62mW$ and for $H = 0, 4.9T$ $A_c \approx 2.1mW$.

Fig. 4.13 shows the spontaneous voltage as a function of the applied radiation's frequency with $10dBm$ at different magnetic fields. At first the different curves seem to be messy and uncorrelated, however when scrutinizing them one can see that many of the features reoccur with different amplitudes and with some voltage shift between the curves. Some of those

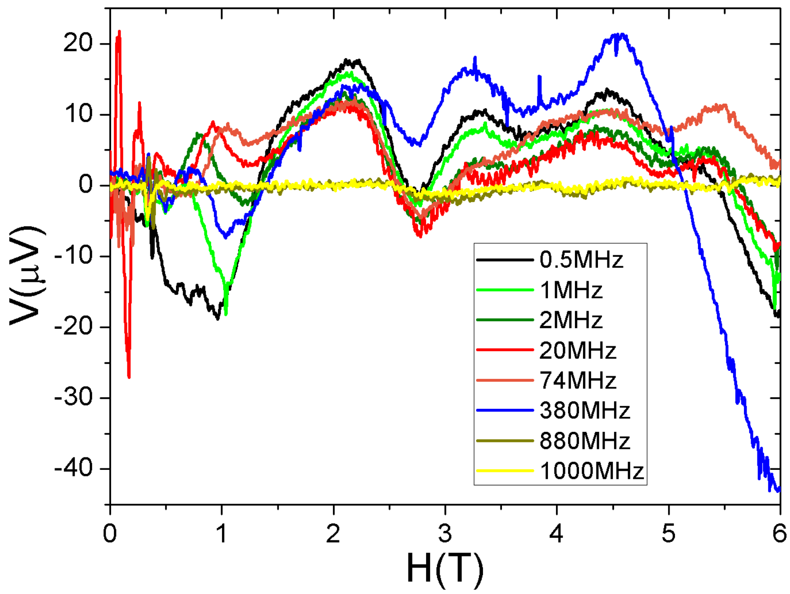

Figure 4.14: *DC voltage along NW14 radiated with a* $10dBm(10mW)$ *at different frequencies as a function of external magnetic field. Green arrows indicate some features that reoccur in all curves.*

features are marked with arrows in the figure. Two main features seem to always appear regardless of the applied magnetic field that may be important to our understanding of this system. One is a segment of zero voltage around $f \approx 300MHz$, and the other is a cutoff frequency, above which the effect seems to disappear, which is about $f \approx 800MHz$.

Fig. 4.14 depicts the spontaneous voltage as a function of magnetic field for different frequencies of the radiation. A few important bits of information can be extracted from this graph. One is the fact that the cutoff frequency is once again observed above $f \approx 800MHz$, so the measurements gives a flat line for frequencies in that range. Another is that the measurement can be separated into two main areas: the low magnetic field regime $H < 0.5T$ where the different curves are somewhat erratic, and the higher field regime $H > 0.6T$, where the different curves distinctly differ from one another but still share many common features.

Chapter 5

Discussion

5.1 Voltage along nanowire

Due to the large amount of data concerning the phenomenon of spontaneous voltage, a short summary of our findings is in order.

At intermediate levels of disorder we observe a spontaneous voltage drop along our nanowires at temperatures below T_c, for no apparent reason (Fig. 4.3). Such a phenomenon, where a voltage drop with no bias applied, seems to contradict the basic law of thermodynamics - there is no free energy in nature. An experiment was performed to check if this phenomenon indeed implies an energy source in our setup (Fig. 4.9), and it was found that energy is indeed generated at a rate of femtowatts. Therefore we were compelled to perform a few experiments to check what unknown bias in our system creates this energy.

A few DC bias sources were checked, such as a current leakage from the measurement devices or a temperature gradient manifesting the Nernst effect. These DC biases were introduced intentionally in an attempt to bolster the effect, and all have failed to affect it (Figs. 4.10 and 4.11).

Alternatively, an AC bias was tested by means of electromagnetic radiation in the experiment chamber and proved to strongly influence the effect (Figs. 4.12, 4.14 and 4.13). A thorough experiment where the effects of frequency, amplitude and magnetic field on the nanowire are tested was successfully performed. Furthermore, it was proved with the aid of a spectrum analyzer that a parasitic radiation always penetrates the chamber, although its source is yet to be found.

It seems at this point that a few results point at an unavoidable conclusion that this effect results from vortex physics which somehow rectifies this radiation. The first indication towards this conclusion is that the effect is only visible below T_c, hence its closely related to superconductivity. Second is the extreme antisymmetry of the voltage in magnetic field, that can be attributed to the vortex-antivortex symmetry.

So the remaining question is what mechanism in our system causes the rectification of supposedly harmonic vortex movement across the nanowire so that they produce a DC voltage along it. A mechanism which we find to fit most of our data is the vortex ratchet effect, which was introduced in chapter 1, however this effect calls for asymmetric pinning centers. In most experiments these were fabricated intentionally and embedded into superconducting films. We will now show how the ratchet effect can be manifested in our nanowires.

As we pointed out in chapter 1, there are many evidences that point at InO thin films as electrically inhomogeneous, and a portion of those evidences is given in chapter 1. This inhomogeneity causes some areas of the thin film to be more prone to destruction of superconductivity than others. When a magnetic field is applied to the sample, these weak superconducting islands turn into normal state islands. These islands may act as pinning sites for vortices.

Once we accept that the existence of pinning sites of some sort in our sample is plausible, and remembering that our nanowire's width is of the order of $50nm$, we can imagine a scenario where there exists a movement of vortices from outside the wire, which can be thought of as a condensate of vortices, into the pinning site and out the other side, as sketched in Fig. 5.1. Such movement would obviously create a voltage drop along the wire, as any vortex flow would.

Such a case, with a time-harmonic force, would cause a time harmonic voltage which will average to zero. However, a case in which the pinning site is asymmetric in shape or if it is positioned at a point that is not at the middle of the wire, the ability of a vortex to move through the nanowire in either direction would be not equal. A sketch of the pinning potential is

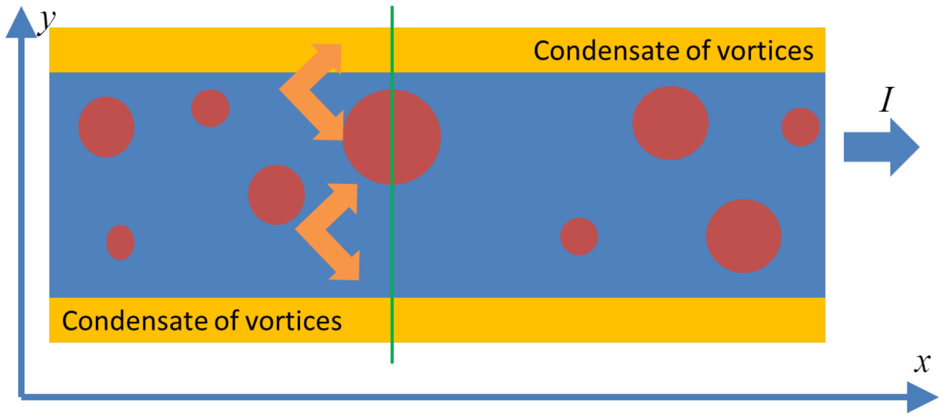

Figure 5.1: *A schematic picture of a nanowire (blue) with scattered pinning sites (red circles). The areas above and below the nanowire act as vortex (yellow) sources, and can be viewed as vortex condensates. Movement of vortices across the wire is possible through a pinning site (orange arrows). The green line marks a cross-section which's effective potential is given in Fig. 5.2.*

given in Fig. 5.2. It shows that when the external force acting on vortices pushes them rightwards, which is the easy direction of travel, vortices flow through the pinning site. When the force pushes them leftwards, a single vortex will get trapped in the pinning site and prevent other vortices from moving in this direction via vortex-vortex repellant interaction.

In the naïve scenario suggested in our framework the entire process is dominated by a single pinning site which contains one vortex at a time. This may not be far from realistic if one considers the fact that the behavior of this vortex movement with size of the barriers is exponential. Due to this

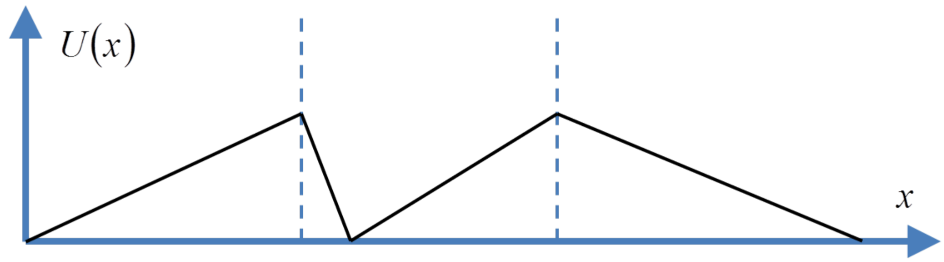

Figure 5.2: *A schematic view of a pinning site in our sample. Entry to the sample is equally easy from either side, however exit is harder in one direction over the other.*

behavior, any case in which the barrier on either side is too large will not contribute to the vortex movement, and if both barriers are too small, they will be negligible when compared to the external force.

A great deal of our data seems to agree with this interpretation of the system. For example, one can distinguish two separate regions in Fig. 4.14, as stated in the text. It seems that above $H = 0.5T$ the different curves share more features and generally behave in a more orderly manner. This can be interpreted as the magnetic field of the first vortex entering the sample. The erratic behavior below this value originates from changes in the morphology of the superconducting condensate and the forming of the normal state islands. Note that this is the same order of magnitude of oscillations shown in Fig. 4.7. Calculating the radius of a vortex from this field in which the first vortex penetrates the film, one winds up with vortices of an approximate radius of

$R_v \approx 20nm$, which corresponds to $\xi \approx 40nm$, close to the value expected from InO [20].

When lowering the disorder, the amplitude of the effect is gradually reduced in Fig. 4.5. This corresponds to making superconductivity stronger around the pinning site, making the barriers higher and slowly inhibiting this effect altogether. High temperatures also decreases the amplitude of this effect, as seen in Fig. 4.6. This corresponds to a reduction of the barriers heights which smoothes out the difference between the two, making flow in either direction more symmetric.

The plateau in the lowest temperatures, seen both in Figs 4.2 and 4.3, signals the onset of movement which is independent of temperature. This may be due to a crossover from thermal activation of the vortex movement to quantum tunneling of the vortices through the barrier. Clearly more work is needed to test this speculation.

The dependence on frequency (Figs. 4.13 and 4.14) implies a cutoff or a rapid decay of the effect with frequency above $f \approx 800MHz$. This also has an important role in the ratchet effect, where the vortex does not have enough time to travel to the edge of the pinning site, and thus remains still in average.

Using this last bit of information, one could estimate the speed of vortices across the nanowires. Assuming that the pinning site's diameter is between the size of a single vortex and the width of the entire nanowire, a vortex would have to travel a distance of $R = 20 - 50nm$ in order to exit the pinning site. Since there is a cutoff of the effect near $f = 800MHz$, one could estimate the vortex' speed v_v as $v_v = Rf = 16 - 40m/s$. These values are well within the range of $1 - 100m/s$ which is suggested by [22] as the range in which the vortices response to the pinning sites is the strongest in their system.

Chapter 6

Conclusion

In this work we presented measurements which were conducted on Indium Oxide nanowire in a disordered state. These samples show an intriguing effect where AC signals are rectified by the nanowires into a DC voltage, below the superconducting T_c. We proposed that the cause of this effect is vortex motion, namely the vortex ratchet effect where vortices have a preferred direction of movement due to an asymmetry of the pinning site, which is generated by the disorder and geometry confinement.

Though this model seems to fit a great deal of our data, more experiments and theoretical treatment are required in order to verify this idea. A few issues to be handled in the future would be the filtration of background noise from our system and conducting measurements with more precise AC signals, an act which will help in quantifying and controlling the effect. Another direction would be to intentionally pattern pinning points in wires for better understanding of the dynamics involved, perhaps explaining the behavior of our system in low magnetic fields.

Our work has shown a remarkable case in which the ratchet effect is spontaneously manifested by an electrical inhomogeneity that naturally occurs in our InO nanowires. In the past it was always necessary to deliberately create a sawtooth potential in order to enforce the vortex movement in a preferred direction.

Many future projects arise in the light of this work. The filtration of the background radiation, achieving a quantitative description of the vortex ratchet effect in our system and using it in the future to probe properties of other SIT cases is just a partial list of our future plans.

Appendix A

Abbreviations

- SIT - Superconductor-insulator transition.
- InO - Indium Oxide
- DOS - Density of (energy) states
- MR - Magneto-Resistance
- RT - Resistance vs. temperature
- VT - Voltage vs. temperature
- RH - Resistance vs. temperature
- VH - Voltage vs. temperature
- FT - Fourier transform

Bibliography

[1] P. Drude, Annalen der Physik *306* (3), 566 (1900).

[2] F. Bloch, Z. Physik *52*, 555-600 (1928).

[3] P.W Anderson, Phys. Rev. *109*, 1492 (1958).

[4] N.F Mott, Phil. Mag. *19* 835 (1969).

[5] A.L. Efros and B.I. Shklovskii, J. Phys. C *8*, L49 (1975).

[6] J. Bardeen *et al.*, Phys. Rev. *106*, 162 (1957).

[7] V.L. Ginzburg and L.D. Landau, Zh. Eksp. Teor. Fiz. *20*, 1064 (1950)

[8] K.Yu. Arutyunova, *et al.*, Physics Reports *464*(1-2), 1 (2008)

[9] Y. Wang, L. Li and N. P. Ong, Phys. Rev. B *73*, 024510 (2006).

[10] M. Vélez *et al.*, J. Magn. Magn. Mater. *320* 21, 2547 (2008).

[11] B. B. Jin *et al.*, Phys. Rev. B *81*, 174505(2010).

[12] V.F. Gantmakher and V.T. Dolgopolov, Phys.-Usp. *53* 1 (2010).

[13] A. Frydman, Physica C *391* (2), 15, 189-195 (2003).

[14] D. Kowal and Z. Ovadyahu, Physica C *468* 4, 322 (2008).

[15] V.F. Gantmakher *et al.*, JETP letters *71* 11, 473 (2000).

[16] Y. Dubi *et al.*, Phys. Rev. B, *73*, 054509 (2006).

[17] B.I. Shklovskii, PRB *76*, 224511 (1007).

[18] D. Shahar and Z. Ovadyahu, Phys. Rev. B *46*, 10917 (1992)

[19] B. Sacépé *et al.*, arXiv:0906.1193v1 (2009).

[20] A. Johansson *et al.*, Phys. Rev. Lett. *95*, 116805 (2005).

[21] M. Zgirski *et al.*, Phys. Rev. B *77*, 054508 (2008).

[22] M. Vélez *et al.*, Phys. Rev. B *65*, 094509 (2002).